Supporting Information

Toughening Elastomers Using Mussel-Inspired Multiphase Design

Xuhui Zhang,[‡a] Jun Liu,[‡b] Zhiyu Zhang,[b] Siwu Wu,[a] Zhenghai Tang,[a] Baochun Guo,*[a] Liqun Zhang*[b]

[‡]Xuhui Zhang and Jun Liu contributed equally to this work*

[a] Department of Polymer Materials and Engineering, South China University of Technology, Guangzhou, 510640, P. R. China.

[b] State Key Laboratory of Organic/Inorganic Composites, Beijing University of Chemical Technology, Beijing 100029, China

Corresponding Author

*E-mail: psbcguo@scut.edu.cn

*E-mail: zhanglq@mail.buct.edu.cn

Experimental Section

Materials: The styrene–butadiene rubber (SBR, styrene content 23.5%) was manufactured by Jilin Chemical Industry Company. cis-1,4 polyisoprene (IR) was purchased from Zeonex. Butadiene rubber (BR) was purchased from Yanshan Petrochemical Co. Sinopec. ENR with an epoxidization degree of 50% (ENR-50) was purchased from Chinese Academy of Tropical Agricultural Science. $FeCl_3.6H_2O$ (analytically pure) was produced by Damao chemical reagent factory. Other rubber additives were industrially available products and used as received.

Elastomer Preparation: Predetermined amount of SBR and ENR were firstly mixed for 5 min in an open two-roll mill, followed by the addition of $FeCl_3$ for another 5 min. Subsequently, the sulfur-based curing package was compounded into the mixture. For all samples, the well mixed compounds were hot-pressed at 160 ^oC with Tc90 (the optimized curing time) to crosslink the elastomers. The formula of the samples with the same curing package is summarized in Table S1.

Method of coarse-grained molecular dynamics simulations: In order to further analyze the reinforcing mechanism, the classical coarse-grained molecular dynamics simulations (CGMDSs) are adopted. To simulate the experimental system, we use the number of 400 and 100 of polymer chains with 100 beads in each chain to model SBR and ENR, separately, as shown in Fig. S9. In the meanwhile, a certain number of larger coarse-grained beads are introduced into the system to model Fe^{3+}.

The non-bonding interaction, including the coordinate interaction formed between ENR and Fe^{3+}, is modeled by the truncated and shifted Lennard-Jones (TSLJ)

potential:

$$U_{ij}(r)=\begin{cases}4\varepsilon_{ij}\left[\left(\dfrac{\sigma}{r-r_{\mathrm{EV}}}\right)^{12}-\left(\dfrac{\sigma}{r-r_{\mathrm{EV}}}\right)^{6}\right]-U(r_{\mathrm{cutof}f}), & 0<r-r_{\mathrm{EV}}<r_{\mathrm{cutoff}}\\ 0, & r-r_{\mathrm{EV}}\geq r_{\mathrm{cutoff}}\end{cases} \quad (1)$$

where r_{cutoff} is the distance where the interaction is truncated and shifted so that the energy are zero, r is the distance between two interaction sites. Here $U(r_{\mathrm{cutoff}})$ is a constant to maintain the continuity of the potential energy. The interaction between Fe^{3+} and ENR is set to be strongly attractive such as $\varepsilon_{\text{Fe-ENR}}=5.0\varepsilon$ and $r_{cutoff}=2.5\sigma$, whose interaction strength is in the range of the coordinate bond based on the mapping standard, while the interaction between Fe^{3+} and SBR is set to be purely repulsive such as $\varepsilon_{\text{Fe-SBR}}=1.0\varepsilon$ and $r_{cutoff}=1.12\sigma$. Meanwhile, to make the well dispersion of Fe^{3+} in the ENR phase, the interaction between Fe^{3+} and Fe^{3+} is set to be repulsive such as $\varepsilon_{\text{Fe-Fe}}=2.0\varepsilon$ and $r_{cutoff}=1.12\sigma$. Note that for the coordinate bond Fe^{3+}-ENR and the interaction Fe^{3+}-SBR, r_{EV} is equal to $\sigma/2$. For the interactions between SBR-ENR, SBR-SBR and ENR-ENR, r_{EV} is equal to zero. For the interaction between Fe-Fe, r_{EV} is equal to $2R_{\mathrm{Fe}}-\sigma$.

To mimic the cross-linked structure, we introduce the covalent bonds only between SBR-SBR, as well as SBR-ENR, which is modelled via the harmonic potential, similar to the bond stretching energy between neighboring beads in a polymer chain:

$$E_{\mathrm{bond}}(r)=1/2k(r-r_0)^2 \quad (2)$$

where k is the stiff constant, r is the bond length and r_0 is the equilibrium bond length. For all simulations we set k and r_0 to be

100 ε/σ^2 and 1.0σ, respectively.

The simulations are performed under the NPT ensemble where the temperature is fixed at $T^*=1.0$ and $P^*=1.0$ via the Nose-Hoover thermostat. Periodic boundary conditions in all three directions are also employed. Meanwhile, the velocity-Verlet algorithm is used to describe the motion of all beads with the time unit $\delta t=0.001t^*$, reduced by the Lennard-Jones time (τ). The number density of the polymer beads is equal to nearly 0.85, ensuring that the system is in the melt state.

The uniaxial tensile deformation is performed by following our previous work.[1, 2] For instance, the box is deformed in the z direction by changing its length from $L_z(0)$ to $L_z(0)\alpha$, while the box length simultaneously shrinks to be $L_z(0)a^{-1/2}$ in the other two directions. And the statistical stress σ in the z direction is derived by the deviatoric tensor, as follows:

$$\sigma = (1+\mu)(-p_{zz}+p) \approx 3(-p_{zz}+p)/2 \tag{3}$$

where the $p=\sum_i p_{ii}/3$ is the hydrostatic pressure and μ represents the Poisson's ratio. For the incompressible elastomeric materials, we set $\mu=0.5$. Meanwhile, the tensile rate, ν is defined as:

$$\nu_{\text{stretch}} = \left(L_z(t)-L_z(0)\right)\cdot L_z(0)^{-1}/\tau = 0.0327/\tau \tag{4}$$

Where $L_z(t)$ stands for the length of the box in the elongated z direction with the time t increasing, and τ is the unit of the time. Meanwhile, the second-order Legendre polynomial is used to characterize the bond orientation as equ (5):

$$\left\langle P_2(\cos\theta)\right\rangle = (3\left\langle\cos^2\theta\right\rangle - 1)/2 \tag{5}$$

where θ denotes the angle between a given bond and the deformation direction. The

possible value of $\langle P_2(\cos\theta)\rangle$ ranges from -0.5 to 1, and the value of 0.5, 1 and 0 indicate a perfect orientation perpendicular to the deformation direction, parallel to the deformation direction and randomly orientation, respectively. All the simulations are carried out by using the large scale atomic/molecular massively parallel simulator (LAMMPS), developed by the Sandia National Laboratories, and some more detailed simulation techniques can be found in our previous work. [3, 4]

To quantify the effect of the number of Fe^{3+}, we systematically vary the number from 0, 50 to 100, corresponding to the concentration of Fe^{3+} ranging from 0, 0.79%, and 1.57%, respectively. It is noted that we set the diameter of Fe^{3+} to be two times of the diameter of each polymer bead (denoted by σ).

Characterization: High-resolution transmission electron microscopy (HRTEM) were performed on a JEM-2100F TEM operated at an accelerating voltage of 200 kV. The energy- dispersive X-ray spectroscopy (EDX) was collected by Oxford Instruments 80mm X-Max system. All the samples are stained with osmium tetroxide. The cryogenically fractured surfaces of elastomers were observed by field emission scanning electron microscopy (FESEM, Nova Nano SEM 430), and corresponding EDX were collected using a Horiba EX-250 spectrometer. Dynamic mechanical analysis (DMA) was performed with a TA Q800 dynamic mechanical analyzer (USA). The tests were carried out under the tension condition, at a frequency of 1 Hz and a strain of 0.5%. The scanning temperature ranged from -80 to 120 °C at a heating rate of 3 °C/min. Tensile tests of elastomers at room temperature were measured using UCAN UT-2060 (Taiwan) instrument with extension rate of 500 mm/min following

ASTM D 412. The loading-unloading cycles were performed by UCAN UT-2060 (Taiwan) instrument with extension rate of 100 mm/min. The toughness (W), characterized by the work to failure, is calculated by the equation (1):

$$W = \int_{\varepsilon=0}^{\varepsilon=\varepsilon_{max}} \sigma d\varepsilon \quad (6)$$

where σ is the stress (MPa), ε is the strain.

The rheological experiment was performed on a rheometer Anton Paar MCR302 (Austria). Strain sweeping measurement was conducted at a constant frequency of 1Hz from a strain of 0.1% to 200%. The stress-relaxation experiments at 25 °C were performed on a TA DMA Q800 machine. The samples were stretched to a 100% strain at the rate of 500% strain per min, and the constant strain was maintained to measure the stress relaxation for 60 min.

Table S1. Composition of samples[a]

Code	SBR (wt%)	ENR (wt%)	FeCl3 (wt%)
Iron-MN-1	88.4	9.8	1.8
Iron-MN-2	78.6	19.6	1.8
Iron-MN-3	68.8	29.4	1.8
Iron-MN-a	79.8	19.9	0.3
Iron-MN-b	79.5	19.9	0.6
Iron-MN-c	79.3	19.8	0.9
Iron-MN-d	79.1	19.7	1.2
Iron-MN-e	78.6	19.6	1.8

[a] rubber ingredients (relative to 100 g of gum): zinc oxide 5 g; stearic acid 1 g; 2-mercaptobenzimidazole 1.5 g; N-cyclohexyl-benzothiazole-2-sulphenamide 1.5 g; 2,20-dibenzothiazole disulfide 0.5 g; sulfur 2.0 g.

Table S2. Mass fraction of C, O, Fe and Zn of the selected areas in Figure 2b counted from EDX scans.

Code	C (%)	O (%)	Fe (%)	Zn (%)
Area 1	88.17±1.03	11.64±0.24	0.19±0.12	0
Area 2	72.30±0.90	16.76±0.28	0.15±0.14	10.79±0.49
Area 3	71.20±1.10	14.58±0.31	1.19±0.16	13.04±0.53

Table S3. Mass fraction of C, O, Fe and Zn of the selected region in Figure S1b counted from EDX scans.

Code	C (%)	O (%)	Fe (%)	Zn (%)
Area 1	93.58±16.53	3.61±3.16	0.28±0.12	2.54±0.43
Area 2	85.27±19.11	10.67±7.73	0.96±0.27	3.09±0.67

Table S4. Detailed mechanical properties of Iron-MN and contrast samples.

Sample	Young's Modulus, MPa	Tensile strength, MPa	Elongation at break, %	100% modulus, MPa	300% modulus, MPa	Work to failure, MJ. m^{-3}
Iron-free HN	3.69±0.21	1.76±0.08	224±12	1.07±0.02	-	2.42±0.22
Iron-HN	3.41±0.27	1.91±0.17	262±17	1.03±0.01	-	3.04±0.27
Iron-free MN	4.22±0.48	3.51±0.23	363±17	1.13±0.04	2.65±0.09	6.28±0.54
Iron-MN	13.72±1.07	13.98±0.58	476±5	2.92±0.18	7.27±0.34	29.95±1.57

Table S5. Detailed mechanical properties of Iron-MN samples with various ENR content (the Iron content is set as 1.8 wt%).

Sample	Young's Modulus, MPa	Tensile strength, MPa	Elongation at break, %	100% modulus, MPa	300% modulus, MPa	Work to failure, MJ. m^{-3}
Iron-HN	3.26±0.08	1.71±0.01	258±7	0.98±0.01	-	2.72±0.07
Iron-MN-1	5.05±0.13	10.61±0.63	659±26	1.28±0.06	3.44±0.17	29.10±2.64
Iron-MN-2	13.69±0.78	11.85±0.13	538±10	2.62±0.11	6.30±0.18	31.98±0.44
Iron-MN-3	44.38±3.03	11.83±0.46	379±15	5.14±0.03	10.00±0.17	27.52±2.00

Table S6. Detailed mechanical properties of Iron-MN with various $FeCl_3$ concentration.

Sample	Young's Modulus, MPa	Tensile strength, MPa	Elongation at break, %	100% modulus, MPa	300% modulus, MPa	Work to failure, MJ. m^{-3}
Iron-free MN	4.22±0.48	3.51±0.23	363±17	1.13±0.04	2.65±0.09	6.28±0.54
Iron-MN-a	4.67±0.12	6.31±0.53	438±11	1.28±0.01	3.29±0.09	11.49±0.85
Iron-MN-b	9.84±0.25	11.66±0.85	447±20	2.47±0.10	6.30±0.10	22.85±1.91
Iron-MN-c	13.72±1.07	13.98±0.58	476±5	2.92±0.18	7.27±0.34	29.95±1.57
Iron-MN-d	17.50±0.82	15.03±0.25	472±7	3.39±0.14	8.25±0.35	33.18±0.33
Iron-MN-e	13.69±0.78	11.85±0.13	538±10	2.62±0.11	6.30±0.18	31.98±0.44

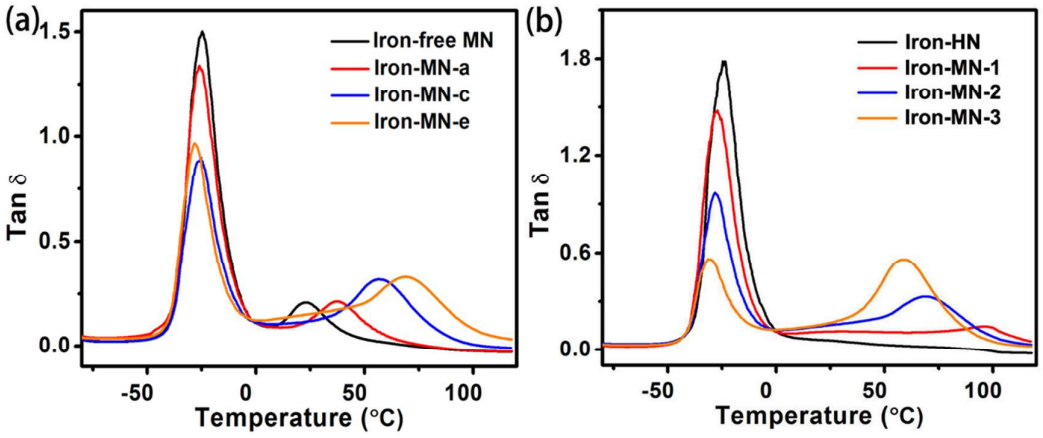

Figure S1. Temperature dependence of loss factor (tan δ) of Iron-MN with various $FeCl_3$ concentration (a) or ENR content (b).

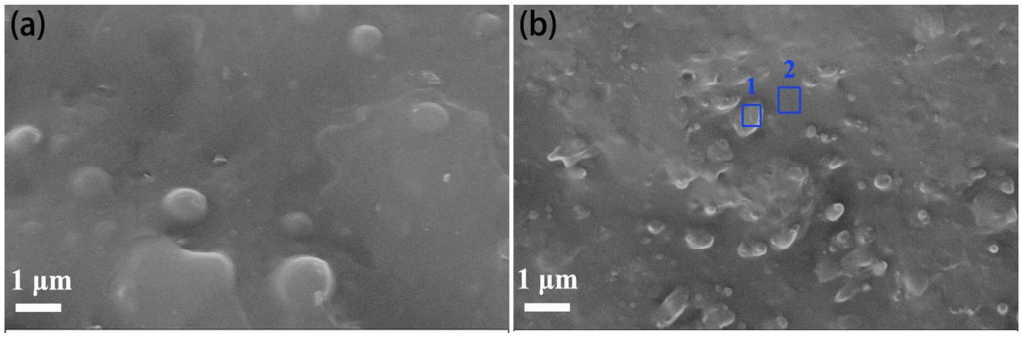

Figure S2. SEM images of Iron-free MN (a) and Iron-MN (b).

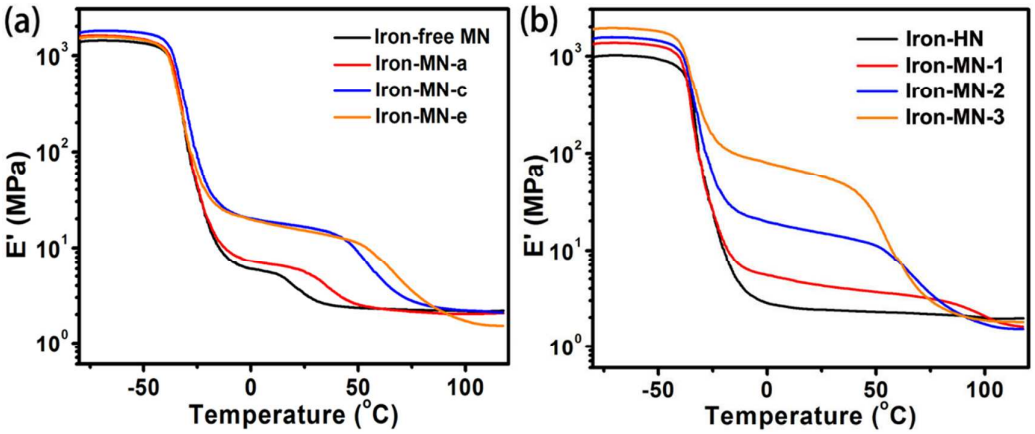

Figure S3. Temperature dependence of storage modulus (E') of Iron-MN with various $FeCl_3$ concentration (a) or ENR content (b).

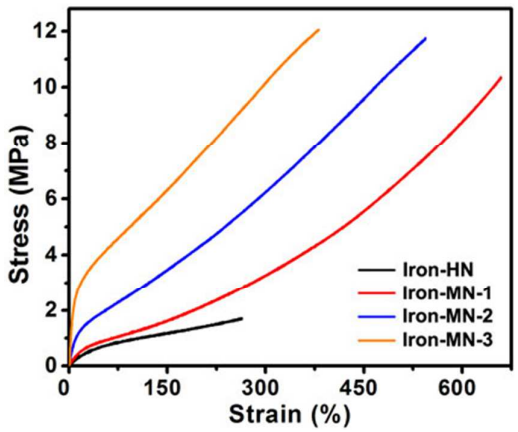

Figure S4. Typical stress-strain curves of Iron-MN with various ENR content (the Iron content is set as 1.8 wt%).

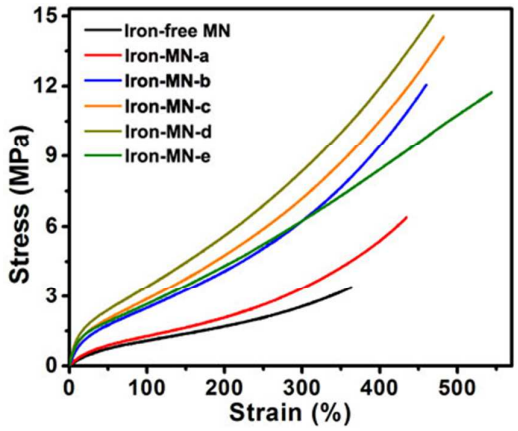

Figure S5. Typical stress-strain curves of Iron-MN with various $FeCl_3$ concentration.

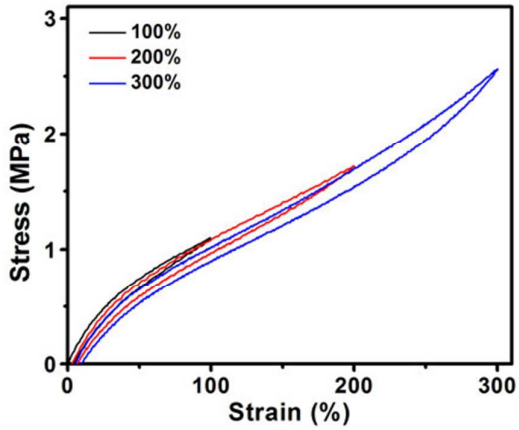

Figure S6. Loading-unloading cycles of Iron-free MN with incremental strain.

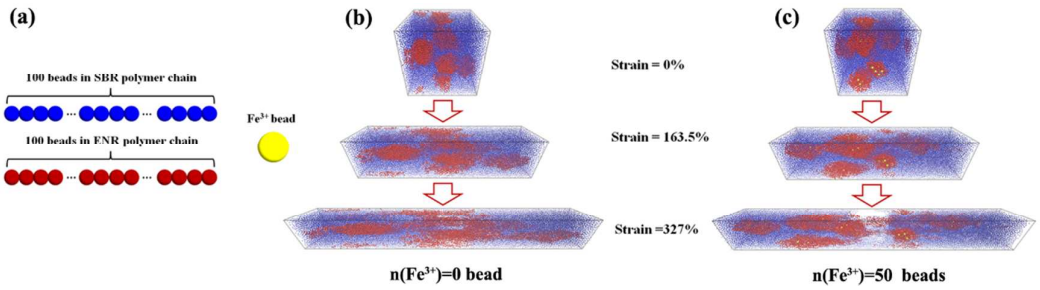

Figure S7. (a) Schematics of the coarse-grained models for SBR, ENR and Fe^{3+}. Snapshots monitoring the deformation process (b) with 0 of Fe^{3+} and (c) with 50 of Fe^{3+}. It is noted that the ENR domains become more deformed at the large strain. The blue points represent SBR phase, the red beads denote ENR phase and the yellow spheres represent Fe^{3+}.

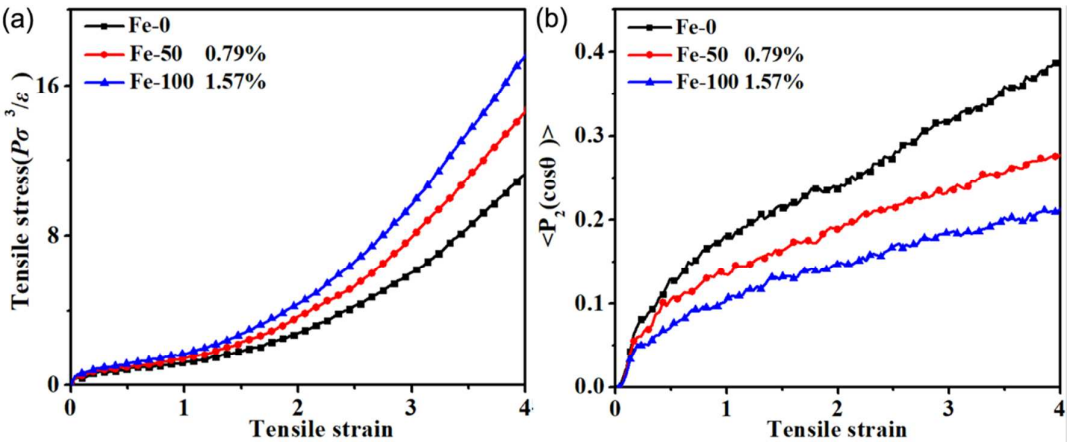

Figure S8. (a) Simulated stress-strain curves of Iron-MN with various Fe^{3+} content (ranging from 0 to 1.57 wt%), in approximately quantitative agreement with the experimental samples; (b) The bond orientation of polymer chains in the dispersed phases as a function of the strain.

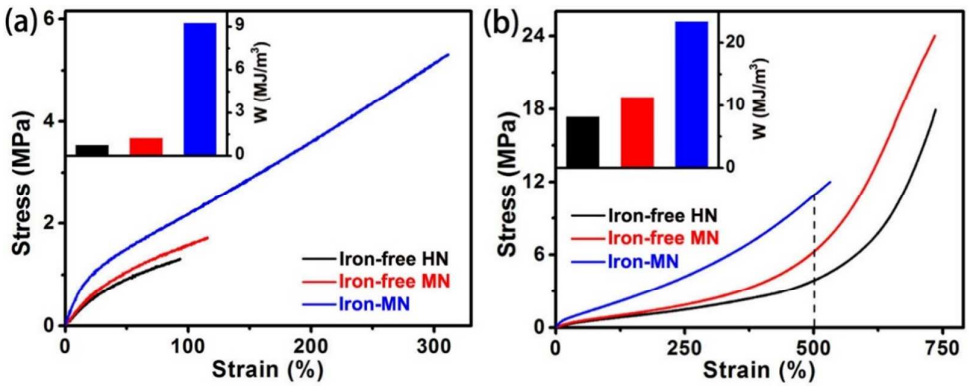

Figure S9. (a) Stress-strain curves of Iron-MN and control samples with BR as the main matrix; the insert is histogram of the work to failure; (b) Stress-strain curves of Iron-MN and control samples with IR as the main matrix; the insert is histogram of the work to 500% strain. The composition of Iron-MN is the same to Iron-MN-c in Table S6.

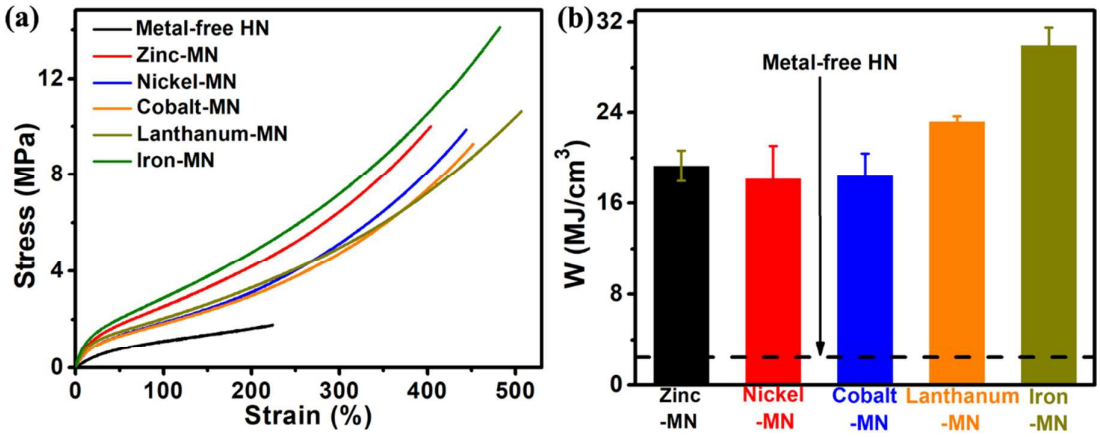

Figure S10. Stress-strain curves (a) and histogram of work to failure (b) of SBR-based MN containing other metal ions (Zn^{2+}, Ni^{2+}, Co^{2+} and La^{3+}). The ingredients are the same to Iron-MN-c.

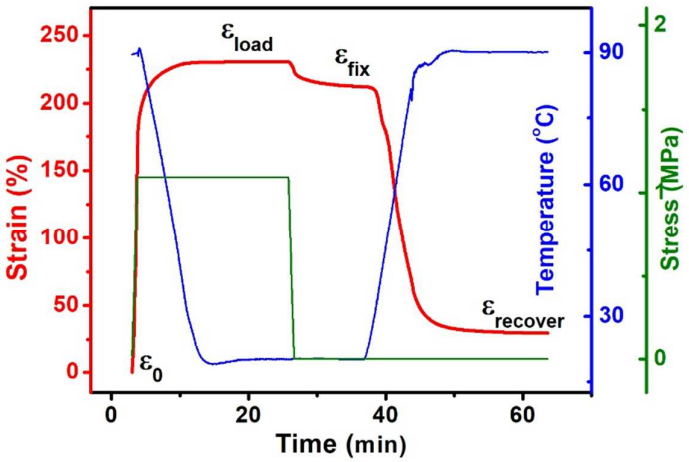

Figure S11. Shape memory effect of Iron-MN-3.

References:

(1) Shen, J.X.; Li, X.; Zhang, L.Q.; Lin, X.S.; Li, H.D.; Shen, X.J.; Ganesan, V.; Liu, J. Mechanical and Viscoelastic Properties of Polymer-Grafted Nanorod Composites from Molecular Dynamics Simulation. *Macromolecules* **2018**, *51*, 2641-2652.

(2) Shen, J.X.; Li, X.; Shen, X.J.; Liu, J. Vanillin-Derived High-Performance Flame Retardant Epoxy Resins: Facile Synthesis and Properties. *Macromolecules* **2017**, *50*, 687-699.

(3) Liu, J.; Zheng, Z.J.; Li, F.Z.; Lei, W.W.; Gao, Y.Y.; Wu, Y.P.; Zhang, L.Q. ; Wang, Z.L. Nanoparticle Chemically End-linking Elastomer Network with Super-low Hysteresis Loss for Fuel-saving Automobile. *Nano Energy* 2016, *10*, 87-96.

(4) Liu, J.; Lu, Y.L.; Tian, M.; Li, F.; Shen, J.X.; Gao, Y.Y.; Zhang, L.Q. The Interesting Influence of Nanosprings on the Viscoelasticity of Elastomeric Polymer Materials: Simulation and Experiment. *Adv. Funct. Mater.* **2013,** *23*, 1156-1163.